



Continuous long-term observations of the carbonate system dynamics in the water column of a temperate fjord



Dariia Atamanchuk^{a,*}, Mikhail Kononets^a, Peter J. Thomas^b, Jostein Hovdenes^c, Anders Tengberg^{a,c}, Per O.J. Hall^a

^a Department of Chemistry and Molecular Biology, Marine Chemistry, University of Gothenburg, SE-412 96 Gothenburg, Sweden

^b Christian Michelsen Research AS, P.O. Box 6031, NO-5892 Bergen, Norway

^c Aanderaa Data Instruments AS, Sanddalsringen 5b, P.O. Box 103, Midtun, NO-5828 Bergen, Norway

ARTICLE INFO

Article history:

Received 15 June 2014

Received in revised form 24 February 2015

Accepted 4 March 2015

Available online 10 March 2015

Keywords:

Carbonate system of seawater

Long-term in situ measurements

pCO₂

Redfield ratio

NPP rates

ABSTRACT

A cabled underwater observatory with more than 30 sensors delivering data in real-time was used to study the dynamics of the upper pelagic carbonate system of the Koljo Fjord, western Sweden, from September to April during two consecutive years (2011–2012 and 2012–2013). In the dynamic upper ca 15 m of the water column, salinity and temperature varied by up to 10 and 20 °C throughout the recorded periods, respectively. Partial pressure of CO₂ (pCO₂), measured with newly developed optical sensors (optodes) at three water depths (5, 9.6 and 12.6 m), varied between 210–940 μatm, while O₂ varied between 80–470 μmol/L. Redfield scaled graphs ($\Delta O_2:\Delta DIC = -1.30$), in which DIC was derived from pH or pCO₂ and salinity-derived alkalinity (A_{Tsal}), and oxygen was measured by the sensors, were used as a tool to assess timing and occurrence of different processes influencing the dynamics of these parameters. Distinctive short-term variations of pCO₂ and O₂ were induced by either tidal oscillations, wind-driven water mass transport in the mixed layer or occasional transport of deep-basin water from below the thermo/halocline to the surface layer. Intensified air–sea gas exchange during short storm events was usually followed by stabilization of gas-related parameters in the water column, such as O₂ concentration and pCO₂, on longer time-scales characteristic for each parameter. Biological processes including organic matter degradation in late summer/autumn and primary production in early spring were responsible for slower and gradual seasonal changes of pCO₂ and O₂. Net primary production (NPP) rates in the Koljo Fjord were quantified to be 1.79 and 2.10 g C m⁻² during the spring bloom periods in 2012 and 2013, respectively, and ratios of O₂ production:DIC consumption during the same periods were estimated to be -1.21 ± 0.02 (at 5 m depth in 2013), -1.51 ± 0.02 (at 12.6 m in 2012) and -1.95 ± 0.05 (at 9.6 m in 2013). These ratios are discussed and compared to previously reported O₂:C ratios during primary production.

© 2015 Elsevier B.V. All rights reserved.

1. Introduction

The global ocean is constantly evolving and changing influenced by natural variability on the short and long-term scales, and by anthropogenic impact. Thus, observational biogeochemical and modeling studies of the oceanic carbon and carbonate system should rely on accurate measurements over extended time periods with high temporal resolution in order to catch and describe the variability. Examples of such studies include the Hawaiian Ocean Time series (HOT/ALOHA, Dore et al., 2009), the Bermuda Atlantic Time Series Studies (BATS, Bates, 2007), the European Station for Time Series in the Ocean (ESTOC, Santana-Casiano et al., 2007) and the Atlantic Zone Monitoring Program (AZMP, Shadwick et al., 2011). Modern observational networks, such as Porcupine Abyssal Plain (PAP) station in North-Eastern Atlantic (Billett et al., 2010; Hartman et al., 2010, 2012) and other

Eulerian observatories, arrays of moorings, floats and buoys have contributed to the understanding of the present state of the global ocean, with respect to e.g. the carbonate system, and facilitated predictions of plausible future scenarios of evolution.

Over the past two decades newly emerging sensor technologies have facilitated large expansion of in situ observations, which led to increased amount of obtained oceanographic data. Furthermore, in situ sensor technologies have opened new possibilities for high-temporal resolution studies of the aquatic environment – otherwise impossible with conventional ship-based water sampling/analysis routines – including oxygen, nutrients and the carbonate system of seawater (e.g. Johnson et al., 2007, 2013).

Several major biological, chemical and physical processes contribute to the dynamics of the carbonate system of seawater such as air–sea gas exchange, vertical and horizontal water mixing, warming/cooling, freshening, CaCO₃ dissolution, photosynthesis, and aerobic/anaerobic respiration. Multi-parameter measurement campaigns with high spatial and temporal resolution can answer the question of which

* Corresponding author. Tel.: +1 902 494 4382.

E-mail address: Dariia.Atamanchuk@Dal.ca (D. Atamanchuk).

of the processes dominate during a chosen period (e.g. DeGrandpre et al., 1997, 1998; Bozec et al., 2006; Zhai et al., 2009), and can provide an efficient approach for studying CO₂ cycling (e.g. DeGrandpre et al., 1995; Körtzinger et al., 2008a,b; Fiedler et al., 2013).

Complete observation of the seawater carbonate system can be achieved by measuring two out of four parameters (dissolved inorganic carbon (DIC), alkalinity (A_T), pH and pCO₂), and the unmeasured parameters can be calculated from the measured ones (Millero, 2007). Direct autonomous in situ measurements of DIC and A_T have been made in a few cases (Byrne et al., 2000, 2002; Wang et al., 2007), while measurements of pCO₂ and/or pH are more common. Thus, DIC required for C-budget calculations is often derived from the measured pCO₂ or pH time-series. In situ pCO₂ observations have been carried out using various technologies based upon measurements of NDIR spectroscopy (Saderne et al., 2013), colorimetry (DeGrandpre et al., 1995) and ion-selective field-effect transistors (ISFET) (Shitashima et al., 2002). Continuous pCO₂ time-series have been successfully recorded with subsmersible instruments and used for the estimation of air–sea CO₂ fluxes and biologically induced changes (Friederich et al., 1995; Hood et al., 1999; Alvarez et al., 2002; Gago et al., 2003; Carrillo et al., 2004; Kuss et al., 2006; Körtzinger et al., 2008a,b). Körtzinger et al. (2008a,b) used observed pCO₂ and salinity-derived measurements of climatological total alkalinity in the calculation of DIC. Although the use of climatology to estimate A_T is justified for the open ocean and deep-water conditions, similar approach might also be applied for the coastal systems, like the one chosen in the present study. River runoff, melting of ice, generally higher variations in nutrient concentrations and contribution from calcareous species may alter alkalinity–salinity dependency throughout the year and bring uncertainty into derived alkalinity values. A significant contribution of organic alkalinity (OA) into A_T during productive season is another important factor that should also be considered and addressed (Muller and Bleie, 2008; Kuliński et al., 2014).

The concept of specific ratios between elements involved in oceanic biogeochemical processes was first described by Redfield (1934). It was postulated that on average, production or respiration of organic matter in the sea involves changes of oxygen and carbon in the molar ratio of 138:106 (1.30). However, further revisions (Anderson and Sarmiento, 1994) suggested that the ratio should be adjusted to 170:117 (1.45) based on experimental data. By observing the Redfield O₂:C ratio over a productive season, the stoichiometry of primary production/respiration expressed by Redfield (1934), Redfield et al. (1963) and Anderson and Sarmiento (1994) can be confirmed or modified (Körtzinger et al., 2008a; Johnson, 2010).

In this paper we report on the dynamics and biogeochemical aspects of the dissolved carbonate system in the Koljo Fjord, western Sweden, and focus on high temporal resolution time-series of in situ pCO₂ (and derived DIC) and oxygen, recorded during the period of September 2011–April 2013. Newly developed fluorescence lifetime based pCO₂ sensors (Atamanchuk et al., 2014) were used for the first time for successful long-term deployments. To our best knowledge it is also the first time such long-term continuous measurements are made in a Scandinavian fjord system. The study showed that with the collected dataset it was possible to find the relationship between DIC and oxygen and establish how various processes influence the concentrations of these parameters. Furthermore, the Redfield model was used as a framework to interpret seasonal variations of the ratio. The measurements of oxygen at multiple levels during the spring bloom period of two consecutive years enabled calculations of net primary production and verifying the obtained data through comparison with earlier values for the area.

2. Instrumentation and methodology

2.1. Study area, the Koljo Fjord

The Koljo Fjord is part of the so called Orust fjord system around the islands of Orust and Tjorn on the Swedish west coast (Fig. 1a).

The Koljo and Havsten fjord chain embraces the north end of Orust. The Koljo Fjord is connected to the Skagerrak through a small and shallow opening (Malo Strommar, 9 m deep) at its southwest end and to the Havsten Fjord through Notesund sill (12 m deep) at the north-east side (see details in Hansson et al., 2013). Above sill level the fjord is characterized by frequent water exchange with the adjacent fjords and physical water properties resemble conditions in Kattegat and change quickly (Andersson and Rydberg, 1988). Below sill level, the residence time of the basin water is long (about 3 years) and water renewal is restricted to rare occasions of exceptional weather conditions, e.g. persistent easterly winds. Otherwise, winds are not strong enough to facilitate mixing of the entire water column: rocky shoreline covered with trees protects the fjord from winds and high waves. The deepest part of the fjord is at approximately 55 m, and the fjord is often anoxic below about 20 m (Nordberg et al., 2001). The stagnant anoxic basin water is fueled by degradation of organic matter and hence is rich in DIC and nutrients. The lack of deep-water renewal facilitates a buildup of DIC in the anoxic part of the fjord from year to year, which is either flushed with next water renewal or is slowly mixed into the upper layers through turbulent mixing at the pycnocline.

Aarup (2002) reports the Secchi depth for the Orust fjord system to be 4.8 ± 2 m with the values of 4–5 m in January–April, which translates into the euphotic zone being 8–10 m deep during early spring when intense primary production commences.

The Koljo Fjord is an example of the particularities of many Scandinavian fjords and an interesting research site in terms of biogeochemical activity. Due to the well-protected location, highly variable and highly dynamic conditions, strong seasonality and high productivity, the Koljo Fjord is also well suited for field testing of new sensor technology. Furthermore, the infrastructure of the cabled observatory gives on-line access to the data and enables observations in real time.

2.2. In-situ instrumentation and measurements

A cabled observatory (Fig. 1) was installed in the fjord (58.22825 N, 11.57400 E) during April 2011 at 42 m depth, and it has been operational at this location since then.

The observatory comprises of an underwater hub, to which up to four separate and independent nodes can be connected. During the period of the study one node was connected, which consisted of a Recording Doppler Current Profiler (RDCP-600) instrument about 1 m above the bottom and a Seaguard® current meter positioned closer to the surface, and connected to a string with 30 vertically distributed sensors measuring oxygen, conductivity/salinity and temperature at multiple levels, and pCO₂ at one level during 2011–2012 and at two levels during 2012–2013 (Fig. 1b and d). RDCP-600 was equipped with sensors for temperature, salinity, pressure/depth, oxygen and turbidity (Fig. 1b); it provided currents including the top centimeters surface current and relative particle measurements at 1 m resolution through the water column. The SeaGuard® string system provided oxygen, conductivity, temperature and pCO₂ data from multiple levels in the water column starting about 8 m below surface where also a single point Doppler Current and Water Level sensors were directly placed on the SeaGuard top plate. The observatory infrastructure was manufactured by Develogic GmbH (www.develogic.de), and all instruments and sensors were from Aanderaa Data Instruments (www.aanderaa.no). Data were recorded every 30 min and presented in near real-time through the website: <http://koljofjord.cmb.gu.se>.

An additional independent shallow mooring system was deployed in October 2012 about 100 m away from the observatory at 5 m depth from the surface. This system comprised of a stand-alone SeaGuard® instrument with connected sensors for currents, oxygen, pCO₂, conductivity, temperature and pressure/wave height. A multiparameter EXO2® sonde from YSI Inc. (www.exowater.com) was strapped to the Seaguard® mooring frame and provided hourly measurements of chlorophyll a, blue-green algae (BGA), fluorescent dissolved organic matter

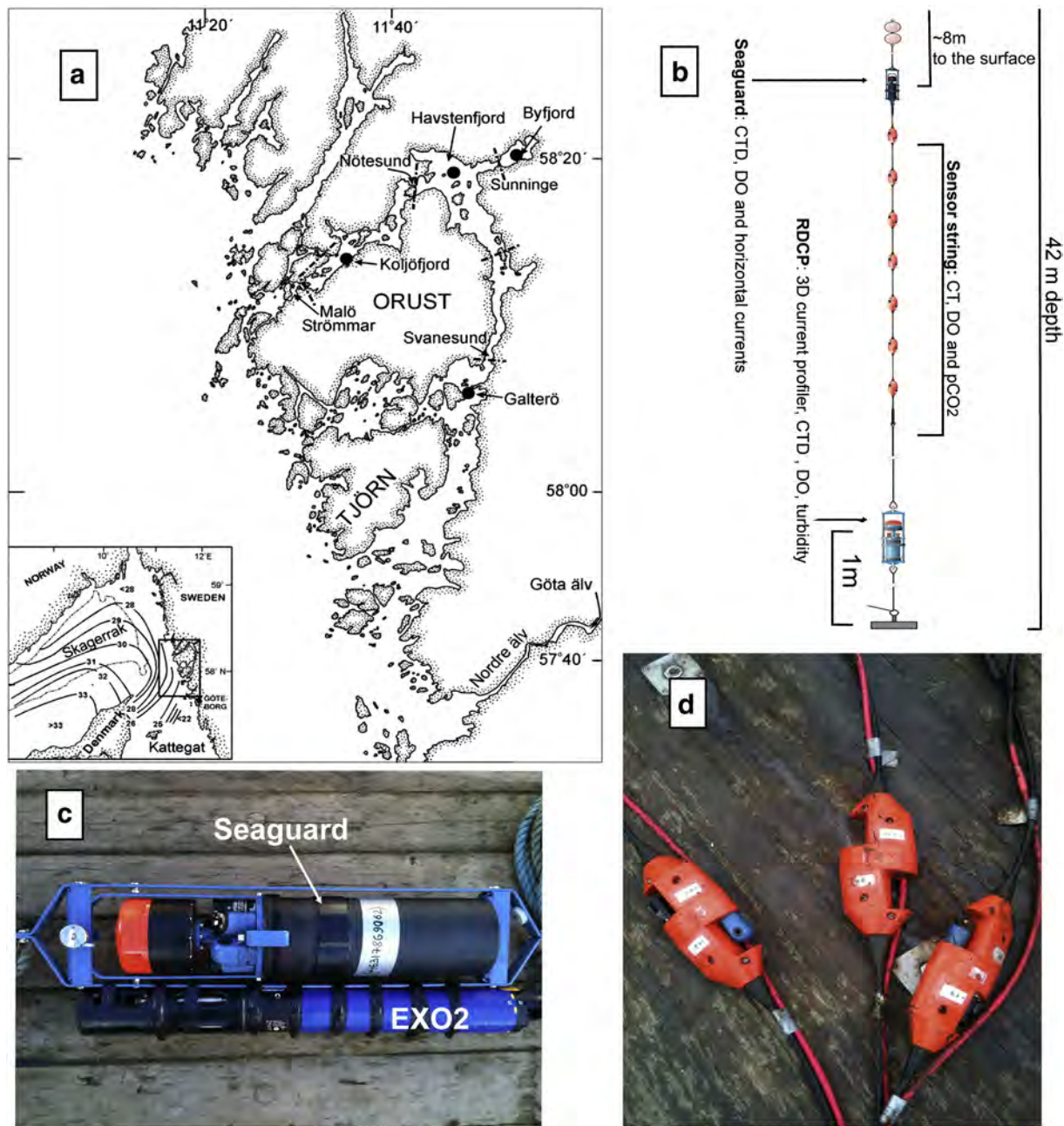


Fig. 1. The Koljo Fjord cabled observatory. (a): Position of the Koljo Fjord in the Orust fjord system (courtesy of D. Hansson). (b): Design and dimensions of the measuring node of the Koljo Fjord cabled observatory used in this study, which consisted of a RDPC and a Seaguard current meter connected to a sensor string (c): View of the shallow mooring installation consisting of the Seaguard® and the EXO2® sonde. (d): View of sensor string pods each of which positioned at a certain level in the water column. Shown installed in the pods are sensors for oxygen and conductivity (left), oxygen and $p\text{CO}_2$ (right), while the center pod is empty.

(fDOM), pH/ORP (oxidation/reduction potential), oxygen, temperature and conductivity (Fig. 1c). For antifouling the latter instrument was equipped with a wiper.

The time-series described in this work covered a seven-month period from September 2011 to April 2012, and a six-month period from October 2012 to April 2013. For the first time period, one $p\text{CO}_2$ optode was placed at 12.6 m depth on the observatory string. During the second period, two $p\text{CO}_2$ optodes were operational and located at 9.6 m depth on the observatory string and at 5 m on the shallow mooring system (Fig. 2). There was no specific reasoning of changing the depth from year to year and the sensors were placed where there were free connections on the sensor string. The technical specifications as well as the strengths and limitations of the $p\text{CO}_2$ optodes used in this study were described in detail in Atamanchuk et al. (2014). Precision of the sensors

varied between 2–10 μatm and the absolute accuracy was set through collecting reference water samples that were later analyzed in the laboratory.

Oxygen/temperature measurements were made using optodes (e.g. Tengberg et al., 2006), models 4835 and 4330 (Aanderaa Data Instruments AS, Norway). Oxygen sensors were mounted either on the string as demonstrated in Fig. 1d or connected to the SeaGuard® top plates (Fig. 1c). In total, oxygen measurements from seven depths were used in the study: 4, 12.8 and 15.8 m in 2012, and 5 (shallow mooring), 8.1, 9.8 and 15.6 m in 2013. Time-series recorded at 5, 9.8 and 12.8 m were combined with $p\text{CO}_2$ /DIC, salinity and temperature at the same depths for the analysis and calculations of co-variance. Oxygen optodes were stable throughout the measurement periods of this study with a field precision of about 0.2 μM and an absolute accuracy of about

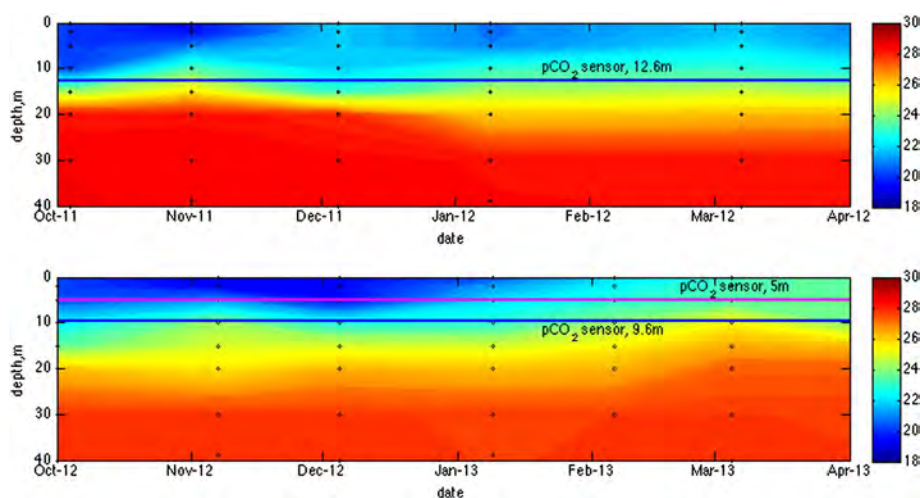


Fig. 2. Salinity contour plot with indication of the depths of recorded $p\text{CO}_2$ time-series in 2011–2013. Dots represent discrete salinity measurements from monthly monitoring program run by SMHI in the Koljo Fjord.

$\pm 2\%$, which was verified by monthly reference water sampling (Fig. 3) and calibration of the sensors in the air. Conductivity/salinity/temperature sensors (model 4319, Aanderaa Data Instruments AS, Norway) were also stable with absolute accuracies of ± 0.05 mS/cm in conductivity, and ± 0.05 in salinity. Temperature was measured with an absolute accuracy of ± 0.05 °C.

Quality control of $p\text{CO}_2$ sensor data is further discussed in below. Notes on the performance of other sensors at the observatory can be found in Friedrich et al. (2014).

2.3. Ancillary data

Ancillary data required for this study, i.e. wind speed and direction, and ambient light information (PAR), was obtained from a nearby meteorological station at the Sven Lovén Centre for Marine Sciences, University of Gothenburg (<http://www.weather.loven.gu.se/data.shtml>).

Water samples for referencing and quality control were collected as well as CTD measurements by SBE 911plus model with Rosette sampler from Sea-Bird Electronics, Inc., <http://www.seabird.com/index.htm>. Sampling was carried out during observatory servicing expeditions using the University of Gothenburg ship R/V Skagerak during December 2011, April 2012, October 2012 and April 2013. Additional reference data for oxygen, salinity and temperature were obtained from the monthly monitoring program that has been operated for many years at this location by the Swedish Meteorological and Hydrological Institute (http://produkter.smhi.se/pshark/datamap_bohuskusten.php?language=s).

High-resolution CTD data were used for validation of interpolated salinity data. Because conductivity sensors could not be placed simultaneously at the same water depth as the $p\text{CO}_2$ and oxygen sensors on the string (see Fig. 1c), the salinity at 12.6 m and 9.6 m was estimated by interpolation of salinity sensor data above and below the $p\text{CO}_2/\text{O}_2$ /temperature sensors. On the shallow mooring, salinity was measured directly at the same depth as the other sensors.

Reference $p\text{CO}_2$ data were used for initial offset adjustment of the sensor readings and for drift validation at the end of the deployments. For the details of adjustment procedure see Atamanchuk et al. (2014). The reference data were calculated from DIC and A_T measurements of water samples. The CO2SYS software was used to compute $p\text{CO}_2$ from the raw data (Lewis and Wallace, 1998). In the calculations we used a set of dissociation constants from Mehrbach et al. (1973) refitted by Dickson and Millero (1987) as suggested by Lee et al. (2000). A_T was measured by potentiometric titration of the bottled samples according to Haraldsson et al. (1997). The titration system gave a precision in order of ± 2 $\mu\text{mol/kg}$ SW. No correction for potential contribution of

OA was made. Determination of DIC was performed by acidification of the samples and stripping with N_2 gas, and analyzing the resulting CO_2 gas with a LiCOR instrument, model Li-6262, LI-COR Inc. (Goyet and Snover, 1993; O'Sullivan and Millero, 1998). The precision of the DIC measurements was $\pm 2\text{--}3$ $\mu\text{mol/kg}$ SW. An absolute accuracy of the DIC and A_T of $\pm 2\text{--}3$ $\mu\text{mol/kg}$ SW for both parameters was obtained by regular calibrations against Certified Reference Material (CRM) supplied by A. Dickson Laboratory, Scripps Institution of Oceanography, USA. Calculation errors in $p\text{CO}_2$ were derived from the errors in DIC and A_T measurements.

2.4. Salinity-derived alkalinity and DIC

By determining water sample salinity and establishing a relation between salinity and measured alkalinity (Lee et al., 2006), we could use salinity time-series as a proxy for alkalinity in e.g. DIC calculations. Errors in $A_{T\text{sal}}$ were estimated as standard deviation (STDEV) of the measured values vs. predicted by the regression model. Model 1 type regression model was created using A_T and salinity data and lsqfit.m MATLAB function taken from <http://www.mbari.org/staff/etp3/regress.htm>.

It was previously shown (e.g. in Muller and Bleie, 2008; Kuliński et al., 2014) that A_T could be overestimated by up to 3.5% when using a classical potentiometric technique for sample analysis due to contribution from OA. Thus, summer values were excluded since they could influence the relationship due to higher contribution of organic alkalinity (OA) in estimations of A_T during highly productive summer season. Taken into account were A_T –salinity data pairs obtained during the same period that the time-series were recorded, i.e. autumn–winter–spring (Fig. 4). Spring values were also potentially biased due to bloom production. The errors associated with overestimation of A_T due to unaccounted contribution of OA are also given and discussed below.

The A_T –salinity relationships were derived from about 85 water column A_T and salinity samples/measurements gathered during expeditions in 2011–2013 from the oxygenated part of the fjord (i.e. above pycnocline). Since no previous carbonate system surveys have been made in this region, we relied exclusively on these relationships.

DIC time-series were calculated using salinity-derived alkalinity ($A_{T\text{sal}}$) and $p\text{CO}_2$ or pH time-series measured with sensors (Fig. 5). Errors (STDEV) associated with this proxy approach to $A_{T\text{sal}}$ as well as measurement errors in $p\text{CO}_2$ /pH and uncertainty in solubility and dissociation constants K_0 , K_1 , and K_2 , were used for assessment of the quality of derived DIC data. Calculation of propagating errors in DIC uses the partial derivatives given in Dickson and Riley (1978).

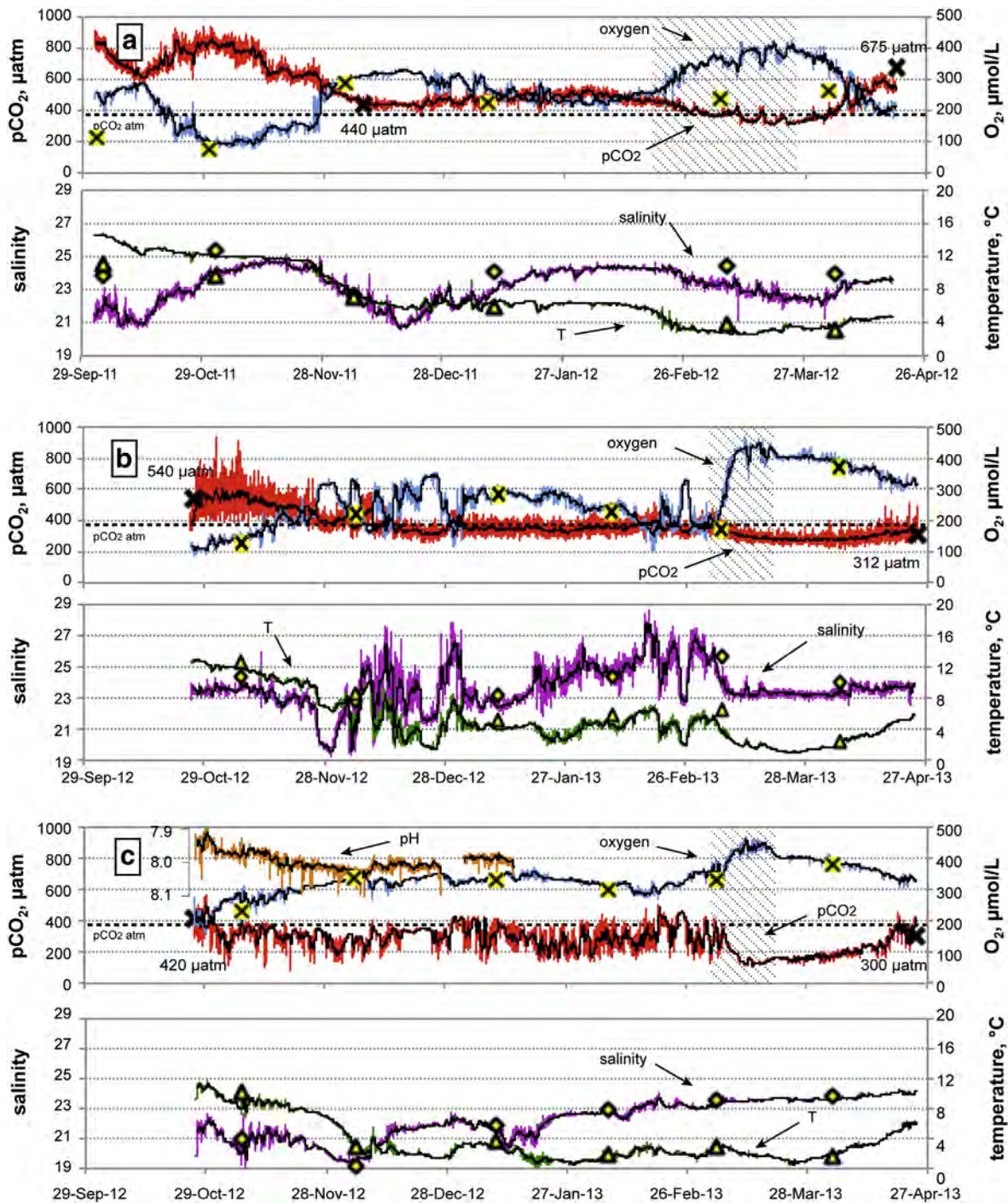


Fig. 3. Recorded $p\text{CO}_2$, pH and oxygen time-series (upper panel), and measured/calculated temperature and salinity time-series (lower panel) for the following periods and depths: (a) October 2011–April 2012, 12.6 m; (b) October 2012–April 2013, 9.6 m; (c) October 2012–April 2013, 5 m. Black line represents a 12 hour averaging of the data; solid black crosses indicate reference $p\text{CO}_2$ data analyzed from collected water samples. Monthly reference data from SMHI: yellow and black crosses are for oxygen; yellow and black diamonds are for salinity; and yellow and black triangles are for temperature. SMHI did not sample at 12.6 m – reference values in a) are given for 15 m depth. Dashed line shows approximate atmospheric $p\text{CO}_2$ level. Shaded areas indicate the periods of spring bloom. (For interpretation of the references to color in this figure legend, the reader is referred to the web version of this article.)

2.5. Production of organic matter (OM) and Redfield ratio concept

In calculations of $\text{O}_2:\text{C}$ concentration ratio during spring periods of intense primary production (spring bloom indicated in Fig. 3), unfiltered O_2 and DIC pair were plotted in a quantity vs. quantity manner. The slope of linear fits to these data indicated searched proportions (Fig. 6). Significance of slopes was assessed by creating a Model II type regression model (lsq cubic.m MATLAB function taken from [http://](http://www.mbari.org/staff/etp3/regress.htm)

www.mbari.org/staff/etp3/regress.htm). This approach helps to assess the model quality by accounting for the errors in X and Y datasets, DIC and O_2 in our case. Errors in DIC were calculated as described above and errors in O_2 measurements were taken from the specified precision of the sensors.

We applied the Redfield concept for visualization of $\text{O}_2:\text{DIC}$ ratios throughout the recorded periods by scaling the axes in the proportion 138:106. Low pass Fourier filtering (>24 h) was also performed on the

calculated DIC and measured oxygen time-series (Fig. 5). This was done in order to filter out short time ‘noise’, which is commonly observed as a result of tidally induced variations. The resulting trends describe the evolution of DIC inventory in relation to corresponding changes in oxygen. The rationale behind using Redfield scaled axis is to visualize the effects of either biological fluxes, mixing, transport of water masses or air–sea exchange on the behavior of O₂:DIC pair rather than quantify the changes or assign the changes to a specific forcing.

2.6. Net primary production (NPP) in spring

NPP rates in the Koljo Fjord were calculated from oxygen time-series recorded by the optodes at the following depths: 4, 12.8 and 15.8 m in 2012, and 5, 8.1, 9.8 and 15.6 m in 2013. The total amount of oxygen produced was calculated as an integrated value in the water column. The following methodology was used: a polynomial fit was applied to the available data points; the resulting fit was extrapolated to the intercept with the x (oxygen production at 0 m depth) and y (the depth where net oxygen production was zero) axes; the resulting areas were integrated to give net oxygen production rates during the spring bloom period in both years. Integrated values were converted to NPP in terms of carbon using the ratio O₂:C = 138:106. The beginning of the spring bloom period was identified from the clear increase of oxygen concentration at 4 m in 2012 and 5 m in 2013. The increase in chlorophyll a concentration at 5 m served as an additional criterion in 2013. Flattening of the oxygen time-series at the depths of 4 m and 5 m in 2012 and 2013, respectively, indicated the end of the spring bloom (Fig. 7).

3. Results

3.1. Data overview

Raw and low pass filtered (>12 hour period) pCO₂, oxygen, salinity and temperature time-series, along with the reference data, are shown in Fig. 3. The first (2011–2012) seven-month time-series (Fig. 3a) was measured with sensors placed at 12.6 m depth on the sensor string. The second (2012–2013) six-month time-series was recorded by sensors located at 9.6 m (Fig. 3b) on the string, and the third at 5 m on the shallow mooring system (Fig. 3c). The measurements at 12.6 m during the 2011–2012 observational period and at 9.6 m during 2012–2013 period laid within similar salinity layer according to Fig. 2, and could be compared with respect to inter-annual variability in the intermediate water layer (Hansson et al., 2013). The measurements at 5 m showed characteristics of the surface mixed layer. The data is summarized in Table 1.

The pH sensor at 5 m depth on the EXO2® sonde recorded variations between 7.88–8.23 during its operational period in October–December 2012 (Fig. 3c).

Table 1

Variations of observed and interpolated (*) parameters throughout the observational periods. Oxygen concentrations marked (†) were measured ca 20 cm below the indicated depth.

Parameter\period	2011–2012	2012–2013	
	12.6 m	9.6 m	5 m
pCO ₂ , μatm	303–937	214–933	95–558
O ₂ , μM	78–425 [†]	86–467 [†]	157–467
Salinity	20.6–25.1*	19.2–28.7*	19.1–24.3
Temperature, °C	2.5–14.6	1.1–13.0	0.5–11.6

3.2. Salinity-derived alkalinity

The A_T–salinity relationship in the Koljo Fjord varied between the 2011–2012 and 2012–2013 observational periods (Fig. 4).

The A_{Tsal} estimated from the A_T–salinity relationship could be described by the following equations:

$$A_{Tsal} = 43.68 \times S + 895.7$$

for the period of September 2011–April 2012 and for the salinity (S) range of 20–26, R² = 0.9709, STDEV = 20.78 μmol A_T/kg SW, and

$$A_{Tsal} = 58.78 \times S + 589.4$$

for the period of October 2012–April 2013 and for the salinity range of 19–27, R² = 0.9679, STDEV = 35.27 μmol A_T/kg SW.

3.3. Primary production in spring

Spring bloom occurred between February 22nd and March 19th in 2012, and between February 27th and March 11th in 2013. The RDCP backscatter values increased significantly during these periods indicating the duration of the spring bloom (Fig. 7a and b). The relative concentration of phytoplankton/particulate organic matter first increased in the photic zone, i.e. 8–10 m according to Aarup (2002), and then gradually in the deeper layers as the particulate matter sank as indicated by arrows in Fig. 7a and b. A fraction of particles seemed to be trapped at the halocline (at about 20 m depth) and did not immediately reach the anoxic zone below. The RDCP backscatter correlated with other parameters like increasing oxygen and decreasing DIC levels (Fig. 7c–e) and direct measurements of chlorophyll a in 2013 (Fig. 7f). At the time of the spring bloom the chlorophyll a concentration at 5 m depth peaked at 70 μg/L and then gradually decreased to levels of 2 μg/L.

3.4. Oxygen and DIC

We observed a negative co-variance between the changes of DIC and oxygen concentrations during each of the two recorded periods (Fig. 5). At the time when the pH sensor was working, DIC was derived both

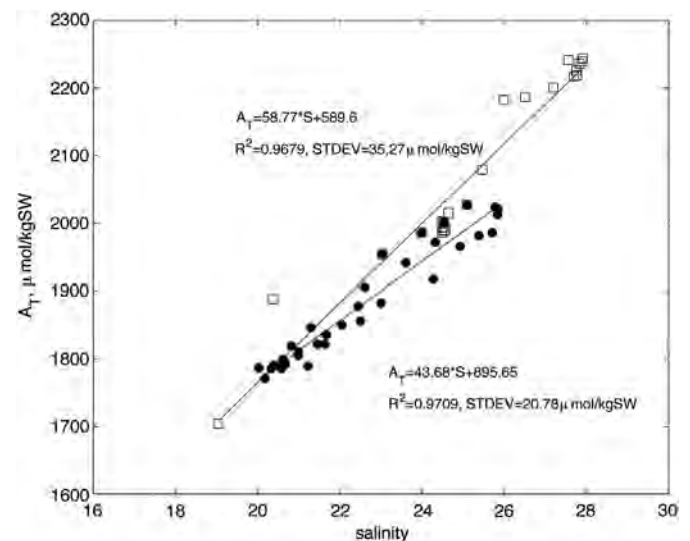


Fig. 4. Established alkalinity–salinity relationship for the water column of the Koljo Fjord. Filled circles (●) represent relationship for the period October 2011–April 2012 and open squares (□) describe the period between October 2012–April 2013. Alkalinity as a function of salinity could be described by the equations indicated in the plot for both datasets.

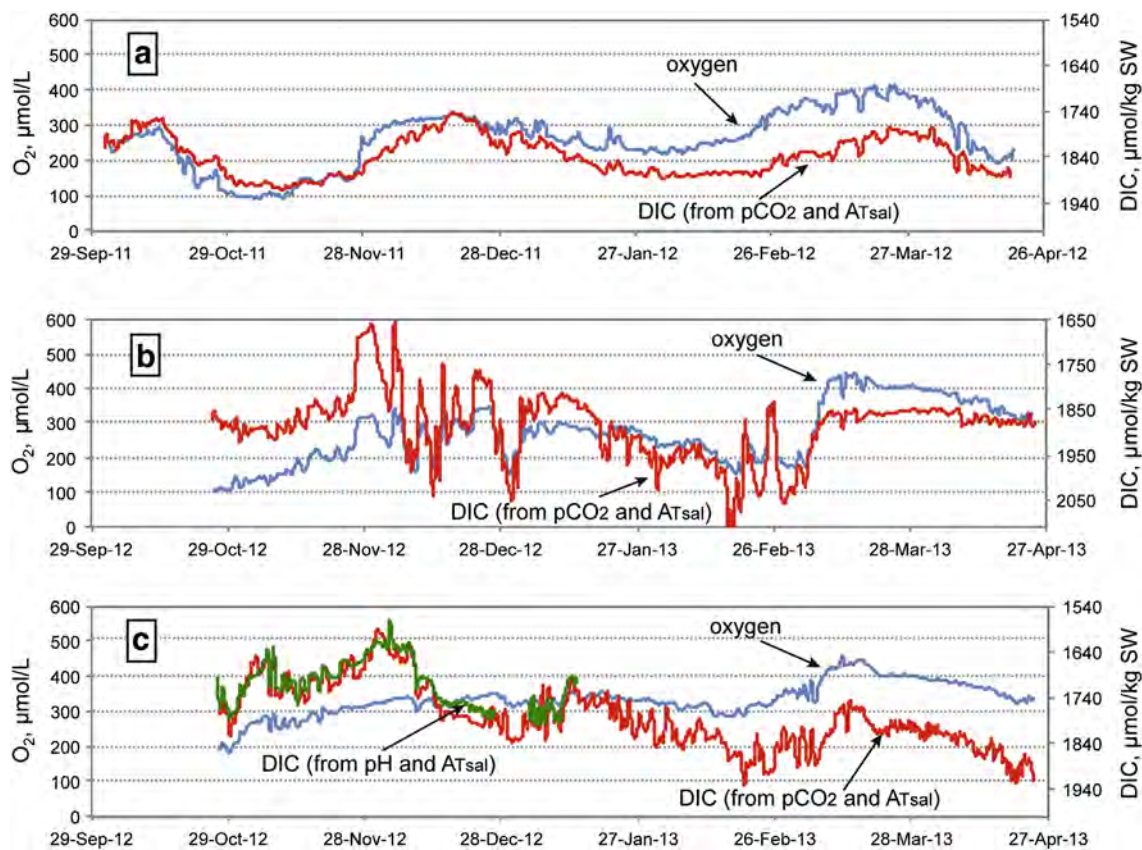


Fig. 5. Coupling between low-pass filtered (>24 hour period) DIC and oxygen time-series data at (a) 12.6 m (2011–2012), (b) 9.6 m (2012–2013) and (c) 5 m (2012–2013). Note: The left and right vertical axes are inverted relative to each other and scaled such that O_2 and DIC data showing variations following the Redfield ratio would be parallel curves. Panel (c) shows an agreement between DIC values calculated from A_{Tsal} and pH (green) and A_{Tsal} and pCO_2 (red). (For interpretation of the references to color in this figure legend, the reader is referred to the web version of this article.)

from the combination of A_{Tsal}/pH and from A_{Tsal}/pCO_2 (Fig. 5c). Calculation error in DIC based on the measurement error in A_{Tsal} , pH and pCO_2 varied between 17–40 $\mu\text{mol}/\text{kg}$. Low-pass (>24 hour period) filtering emphasized long-term trends and the difference in system dynamics at different depths. In the intermediate mixed layer (5–15 m), DIC varied between 1740–1915 $\mu\text{mol}/\text{kg}$ in 2011–2012 (Fig. 5a), while in 2012–2013 the oscillations were more intense and spanned between 1650–2120 $\mu\text{mol}/\text{kg}$ (Fig. 5b). The surface water was generally lower in DIC than at intermediate depth, and covered the range of 1590–1935 $\mu\text{mol}/\text{kg}$ at 5 m depth.

The ratio of absolute change in concentration between O_2 and DIC ($\Delta O_2/\Delta DIC$) during the spring bloom was calculated from slopes (Fig. 6). The molar ratios and the corresponding errors were -1.21 ± 0.02 , -1.51 ± 0.02 and -1.95 ± 0.05 for the 5, 12.6 and 9.6 m depth. Two distinctive regions for the data at 9.6 m depth were observed. The region covering the lowest oxygen concentrations more closely followed Redfield stoichiometry (-1.07 ± 0.04), while the other region showed a higher accumulation of oxygen than expected (-13.34 ± 1.08). A similar, but inverse pattern was seen at 12.6 m: the higher oxygen concentration region showed closer to known stoichiometry (-1.38 ± 0.02), while the other section of the time-series showed the ratio -7.43 ± 0.40 .

3.5. Net primary production

NPP rates calculated from oxygen production were estimated to be 1.79 g C m^{-2} and 2.10 g C m^{-2} during the spring bloom in 2012 and 2013, respectively. Integrated PAR data indicated 25% higher light intensity per productive day in 2013 compared to the previous year.

4. Discussion

4.1. pCO_2 sensor performance

This work provides the first successful continuous combined long-term datasets of pCO_2 (DIC) and multilevel O_2 acquired in Scandinavian fjords. pCO_2 was measured with the newly-developed optodes. The accuracy of these sensors was set by in situ adjustment from analyzing water samples taken at the time of deployment. Adjustment method, which utilizes a pre-deployment calibration and a reference point, allows for compensating for the conditioning-related drift of the sensors (Atamanchuk et al., 2014). Especially at intermediate depths the environment is dynamic with rapid changes in all the measured parameters. It can consequently be challenging to collect representative water samples. The offset between 5 and 75 μatm after 6 and 7 months of deployment shown by the sensors at 9.6 and 12.6 m depths respectively, was attributed partly to the sensor drift and partly to the uncertainty (error) in sampling and/or calculating pCO_2 from the water samples. Errors in the calculation of pCO_2 from sampled DIC and A_T had given an uncertainty in ± 16 –35 μatm , which is a large fraction of the measured offset. The reference samples for comparison were taken at the end of spring bloom (Fig. 3, black crosses on pCO_2 time-series). Thus, unaccounted contribution of OA to A_T would result in overestimation of A_T , which might cause an additional significant bias in pCO_2 calculations. The results from potentiometric titrations and comparison to the calculated values – a method to quantify OA – indicated an additional 12–18 $\mu\text{mol}/\text{kg}$ SW term to A_T at the end of spring bloom (Muller and Bleie, 2008). These numbers were discovered for the surface waters of the Norwegian fjord surface waters, however the resemblance of DIC and A_T changes during the bloom allowed us to assume close or similar

values for the Koljo Fjord. The uncertainty associated with OA in the calculated $p\text{CO}_2$ would have been $\pm 24\text{--}75 \mu\text{atm}$.

No post-deployment examination of the sensors was made, which makes speculations on the actual drift of the sensor unsubstantiated. The authors used secondary arbitrary criteria like the dynamic range and co-variance with the trustworthy oxygen data from the optodes to conclude that the recorded $p\text{CO}_2$ data were of good quality. For the merit of this study it should be mentioned that all acknowledged errors in the measurements were included in the calculations. For instance, the field precision varied between the $p\text{CO}_2$ sensors from $2 \mu\text{atm}$ to $10 \mu\text{atm}$, and the variation was related to differences in electronics and sensing foils of the optodes.

4.2. Carbonate system and oxygen dynamics

Assessment of the dynamics of the carbonate system in the water column and calculations of $\text{O}_2:\text{C}$ ratios for the spring bloom were made through deriving DIC from $p\text{CO}_2$ time-series (Fig. 5). The errors in DIC propagated from a) uncertainty of A_T estimation using salinity as a proxy, b) precision of $p\text{CO}_2$ measurements, and c) uncertainty in equilibrium constants within the carbonate system. The assessment of the dynamics in this study however relied on the relative change of DIC as opposed to the corresponding change in O_2 . In this context, the calculation errors played a minor role, as they would reflect an error in the absolute DIC value.

Besides calculating DIC data from the $p\text{CO}_2$ sensors and alkalinity, pH data were recorded for a three month period at the shallow mooring in 2012, which allowed comparison of the DIC results obtained with two independent methods $p\text{CO}_2/A_{T\text{sal}}$ and $\text{pH}/A_{T\text{sal}}$. The disagreement between these two independent methods was $13.2 \pm 20.1 \mu\text{mol}/\text{kg}$ and both time-series tracked each other well (Fig. 5c) confirming, and verifying the observed dynamics.

The highest values of DIC corresponded to the periods after remineralization of residual particulate organic matter (POM) from the “active season” which occurred in autumn and just before the spring bloom started, when winter storms had induced mixing from deeper suboxic/anoxic carbon rich layers. Winter periods are usually stormy in this area, which also create conditions (Hansson et al., 2013) when DIC rich water from the adjacent fjords can enter the Koljo Fjord basin by spilling over the sill.

The lowest oxygen levels occurred in autumn, when the temperature in deeper layers was relatively elevated and most of the organic matter had been oxidized as reflected by low acoustic backscatter signals measured by the RDCP (data not shown). The highest levels of oxygen occurred during the spring blooms. Periods of intensified primary production were identified from the data (Fig. 3) and would typically lead to 115–120% oversaturation in the upper layers.

The magnitude of variations of DIC and O_2 in the intermediate depth layer was significantly higher during the 2012–2013 period than the previous year (Fig. 5), which was reflected also in the salinity and temperature profiles (Fig. 3). With a few exceptions of intensified air–sea exchange, the consistent negative coupling between oxygen and DIC (Fig. 5a, b) indicated that water masses were entrained at this depth. In the scenario when the upper water column (down to 15 m) was well mixed the oxygen levels would stay close to saturation and would not show such dramatic variability.

During 2012–2013 surface waters were well mixed. $p\text{CO}_2$ and O_2 values were closer to 100% saturation with atmospheric values (Fig. 3c), and DIC was generally lower (Fig. 5c).

Oversaturated levels of oxygen (up to 160% saturation), lower and decreasing DIC values, high chlorophyll a concentrations and a high RDCP signal strength suggest that the spring bloom lasted for 25 days in 2012 and 13 days in 2013, and started in mid-February in 2012 and late-February in 2013. The corresponding starting dates reported from satellite images for the open Skagerrak, outside the fjord, was at the latest on February 28 in 2012 and on March 13 in 2013 (www.smhi.se).

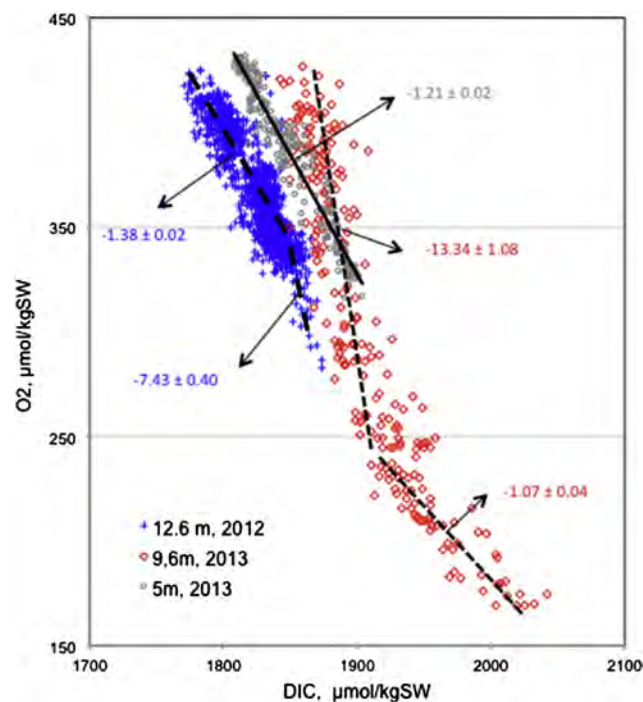


Fig. 6. Correlations between concentrations of DIC and oxygen during primary production in spring (February–March) of 2012 and 2013. For the data at 9.6 m and 12.6 m depth, two different regions showing distinct $\text{O}_2:\text{DIC}$ variations were identified: linear fits to each region are shown as dashed lines. Values for $\Delta\text{O}_2:\Delta\text{DIC}$ ratios are indicated.

A later start of the spring bloom in the open Skagerrak than in adjacent protected fjords is common (B. Karlson (SHMI), pers. comm.). Clear diurnal cycles of primary production/degradation coupled to sunlight were observed from oxygen and $p\text{CO}_2$ data at 5 m depth during spring 2013 (data not shown). The RDCP signal strength data indicated the production of algae in the upper layers during the spring blooms, and a subsequent sinking of particulate matter (most likely POM) down from the photic zone (Fig. 7a and b).

4.3. Redfield stoichiometry

Biological activity (primary production, respiration) should lead to uptake/release of DIC and production/consumption of oxygen in the Koljo Fjord, which should be reflected in simultaneous and proportional changes in the concentrations of these solutes. Specifically, DIC and oxygen time-series plotted on separate axes that are relatively inverted and scaled using the stoichiometry 1:1.3, should result in parallel curves for the two variables if the assumption expressed by Redfield stands (Fig. 5). In practice this approach points at whether biological processes dominate over other processes, rather than confirm/deny ‘Redfieldish’ behavior. To assess the stoichiometry, a property–property plot of DIC vs. oxygen is useful. In Fig. 5a the parallel O_2 and DIC curves indicate that the spring bloom (biological component) dominated in February–March. A rapid increase in O_2 followed by a slower equilibration of the carbonate system during a stormy period at the end of November and through December point at the onset of an air–sea exchange event. Later there was a sign of DIC rich water input (turbulent mixing, water advection) in January and before the spring bloom in February. Higher variability in 2012–2013 made the analysis of processes more challenging (Fig. 5b). While there was a strong signal of biological production in spring, during winter we observed a general enrichment of the water masses in DIC on the background (see 4.5 Water transport and air–sea exchange). Note that sharp and high amplitude spikes in DIC and O_2 through December–beginning of January are less pronounced at 5 m (Fig. 5c) indicating their probable origination from the mixing in at the pycnocline from the deep anoxic basin.

The beginning of primary production in the fjord was associated with increased light availability and production was observed at depths in the suggested photic zone, e.g. down to 8–10 m, but not at 15.6 m in the spring of 2013. However, a clear indication of biological activity in spring 2012 at 12.6 m and very weak biological signal from the optode at 15.8 m implied deeper photic zone (ca 13–15 m) than the suggested in Aarup (2002) using Secchi depth measurements.

Relative amount of particles and chlorophyll a concentration served as additional criteria to select the periods of primary production for each year (Fig. 7). A higher, with respect to the known -1.30 (Redfield) and -1.45 (Anderson), ratio calculated from the 9.6 m time-series in 2012, i.e. -1.95 ± 0.05 , indicated an additional source of oxygen at this depth

apart from primary production. This, we believe, could be a turbulent diffusive transport from the upper layers, where higher light availability, rapid onset of the bloom and lack of ventilation may have facilitated oversaturation of the water with respect to oxygen. The bloom at 9.6 m commenced in -1.07 ± 0.04 proportions and the arrival of oxygen was seen some time in the middle of the bloom resulting into accumulation of oxygen with respect to the consumption rates of DIC. At that time more productive surface layer became oversaturated and outsourced O_2 to the deeper layers. Since we excluded air–sea gas exchange by our assumptions, an underestimation of O_2 :DIC production/consumption ratios in the fjord is expected, especially with respect to the surface layers.

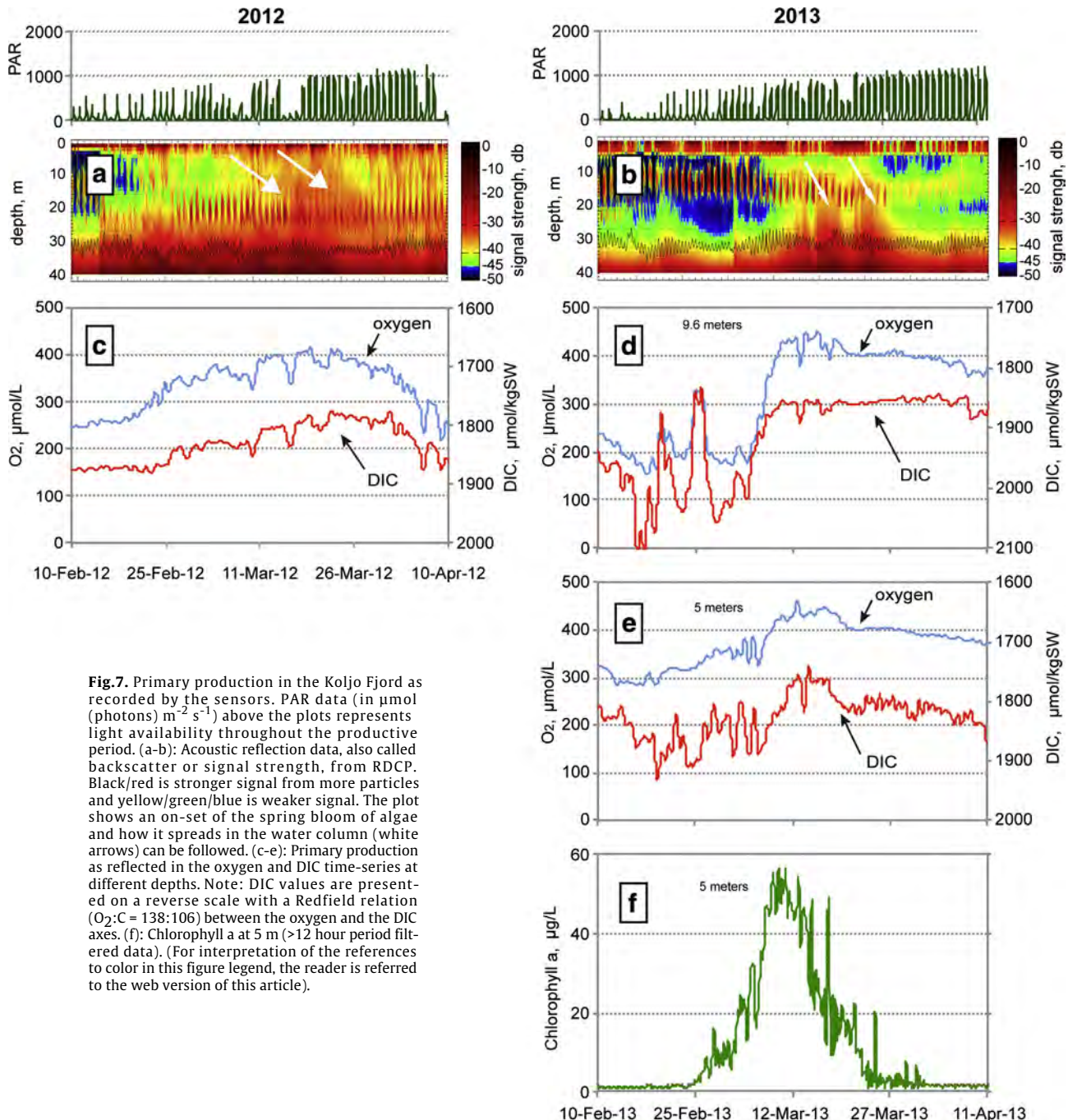


Fig. 7. Primary production in the Koljo Fjord as recorded by the sensors. PAR data (in $\mu\text{mol photons m}^{-2} \text{s}^{-1}$) above the plots represents light availability throughout the productive period. (a–b): Acoustic reflection data, also called backscatter or signal strength, from RDCP. Black/red is stronger signal from more particles and yellow/green/blue is weaker signal. The plot shows an on-set of the spring bloom of algae and how it spreads in the water column (white arrows) can be followed. (c–e): Primary production as reflected in the oxygen and DIC time-series at different depths. Note: DIC values are presented on a reverse scale with a Redfield relation ($O_2:C = 138:106$) between the oxygen and the DIC axes. (f): Chlorophyll a at 5 m (>12 hour filtered data). (For interpretation of the references to color in this figure legend, the reader is referred to the web version of this article).

The analysis of DIC vs. O_2 plot at 12.6 m in 2012 revealed that the primary production commenced on a background of raising DIC, which originated from winter mixing seen as series of spikes in Fig. 5a. Hence an abnormally high ratio -7.43 ± 0.40 could be expected. After the biological component became dominant, the ratio balanced around -1.38 ± 0.02 . Unlike in 2013, we did not observe a distinctive diffusive transport of oxygen from the upper layers.

4.4. Net primary production in the Koljo Fjord

The difference in integrated spring bloom NPP rates in 2012 and 2013 (1.78 and 2.10 $g\ C\ m^{-2}$) was presumably caused by 25% higher light intensity in 2013 in comparison to 2012 based on PAR data (Fig. 7). When normalized to the light intensity value in 2013, and assuming that NPP is proportional to light intensity, the NPP rates during the two spring blooms became more similar (2.23 $g\ C\ m^{-2}$ in 2012 and 2.10 $g\ C\ m^{-2}$ in 2013). The calculated NPP rates are similar or at the lower end in comparison to some previously published values for this area. In the present study NPP rates are given for the period of the spring bloom, which covered the end of February–middle of March, while numbers in the literature often represent NPP estimated for each month separately. For the open Kattegat, Stigebrandt (1991) modeled NPP rates of 2.5 $g\ C\ m^{-2}\ month^{-1}$ and 14 $g\ C\ m^{-2}\ month^{-1}$ in February and March, respectively, based on monthly monitoring data of oxygen. The estimates given in Lindahl et al. (2009) for the Gullmar Fjord, an adjacent fjord which to a great extent has conditions similar to those in the Koljo Fjord, are 7.98 $g\ C\ m^{-2}\ month^{-1}$ in February and 19.41 $g\ C\ m^{-2}\ month^{-1}$ in March. However, the latter numbers are based on daytime incubation data and light index correction, and they could hence be overestimated due to unaccounted difference in respiration rates during day and night. Daily production rates in the open Kattegat in early March at the same latitude as the Koljo Fjord are 93 – 199 $mg\ C\ m^{-2}\ d^{-1}$ according to Heilmann et al. (1994). These rates agree well with those calculated in this study (on average 161 $mg\ C\ m^{-2}\ d^{-1}$ during the spring bloom in 2013). During the 2012 spring bloom the net daily production rate in the Koljo Fjord was lower, on average 71 $mg\ C\ m^{-2}\ d^{-1}$, but the difference between 2012 and 2013 could be explained by a less intense and longer spring bloom period in 2012.

The difference between the NPP rates measured during the spring bloom period in this study (71 – 161 $mg\ C\ m^{-2}\ d^{-1}$), and those previously estimated for this area (89 – 451 $mg\ C\ m^{-2}\ d^{-1}$ (Stigebrandt, 1991), 93 – 199 $mg\ C\ m^{-2}\ d^{-1}$ (Heilmann et al., 1994) and 285 – 625 $mg\ C\ m^{-2}\ d^{-1}$ (Lindahl et al., 2009)) is likely due to differences in methodology used for the calculations in each study, and/or differences temporal in environmental characteristics between the open Kattegat and the enclosed fjords. Each of the procedures utilized in the studies above to estimate NPP has weaknesses and limitations, and includes assumptions. In our study, they are:

- We treated $1\ m^2$ of the water column as a box and assumed that net primary production in the fjord at a certain depth took place at equal rates over the entire fjord. In this way, the horizontal transport of water masses as a bias to the box model was excluded.
- Turbulent diffusive transport of oxygen out of the photic zone to deeper layers was also neglected. However, this transport contributed to the budget calculations anyway since integration was done over the entire water column above the pycnocline, and hence this should not have caused a large error.

Air–sea exchange calculations were impossible in our study due to lack of oxygen and wind speed data at the very surface of the fjord. However, we assumed that air–sea exchange, which gives underestimated NPP values if not being considered, was to some extent counteracted by decreased primary production rates due to exposure to intense UV-light near the surface. Furthermore, air–sea exchange

during the spring bloom periods in 2012 and 2013 was limited due to the weak wind and low wave activity as discussed above.

4.5. Water transport and air–sea exchange

Wind forcing is responsible for 40% of the supplied energy for deep-water mixing in the Koljo Fjord (Hansson et al., 2013). The deep-water mixing is mainly due to internal waves, which are created by barotropic tides across the sill, and cause weakening of stratification throughout the water column (Hansson et al., 2013). Hence wind induced mixing in autumn/winter dominates over other drivers, when biological signals are weak. In addition, air–sea exchange is highly dependent on the wind speed (Wanninkhof, 1992; Wesslander et al., 2011). Coupling between wind and the dynamics of the entire water column was in this study observed as high amplitude oscillations of the measured parameters during the 2012–2013 winter season, when wind speeds were higher in comparison to the previous winter season.

Active exchange of water masses with the adjacent Havsten Fjord and Kattegat usually occurs above sill level. Inflowing dense water is entrained in the intermediate layer of the Koljo Fjord due to steep density gradients and does not reach the deep basin. Unless favorable winds dominate, and lead to turbulent mixing due to internal waves at the pycnocline, the stratification in the fjord remains established and only diffusive processes take place.

Disproportional changes in O_2 :DIC as illustrated in Fig. 5 were observed mainly during winter periods when physical forcing was dominating. Vertical water mixing was always resulting in higher DIC variations than what is expected from Redfield proportions. Accumulation of DIC took place until the primary production period began and decreased the DIC levels. Horizontal transport of water masses altered the concentration levels, but this process sustained a stable O_2 :DIC ratio. This was highly applicable for the intermediate layer (Fig. 5a, b), where the time-series in general tracked each other (horizontal transport), but showed a few occasions of distinctive mismatch and changed O_2 :DIC ratios (vertical mixing).

The fjord is well protected from all directions by narrow and shallow straights and by tree-covered islands. Consequently no ocean waves can reach this area and wind driven waves are small. Apart from occasional waves caused by passing ships/boats, the wave height and tide sensor on the Seaguard® registered several periods with duration up to one week of elevated wind-related wave activity. During these periods, typical wave heights reached only 10–20 cm. On two distinct occasions strong winds and wave action led to the onset of air–sea exchange (Fig. 8).

The combination of wind, wave height and acoustic current measurements spanning the entire water column served to single out these periods. Over a five day period in November–December 2011 oxygen concentrations at 12.6 m depth were ramped up from about 150 to 300 $\mu mol/L$, corresponding to an increase from about 45% to 80% air saturation (Fig. 5a). This period corresponded to a winter storm that induced air–sea gas exchange and vertical mixing (Fig. 8). After the storm oxygen was stabilized over a 1-day period. Slower response of the carbonate system to the air–sea exchange was anticipated, and the measured time lag was approximately 14 days. This number is in-between lag estimates for the Baltic Sea of 3.2 days (Wesslander et al., 2011) and 20 days for typical ocean conditions (Emerson and Hedges, 2008).

Another distinctive wind induced air–sea exchange took place just after the peak of the spring bloom in 2013. It primarily affected the surface layer, and resulted in a lowering of the O_2 supersaturated water to 100% saturation and a slight uptake of CO_2 from the atmosphere (Fig. 5c). This gas ventilation event was not as rapid and intense as during winter 2011, but nevertheless it also affected O_2 concentrations measured at the 9.8 m level (Fig. 5b) indicating a diffusive link between the two depths.

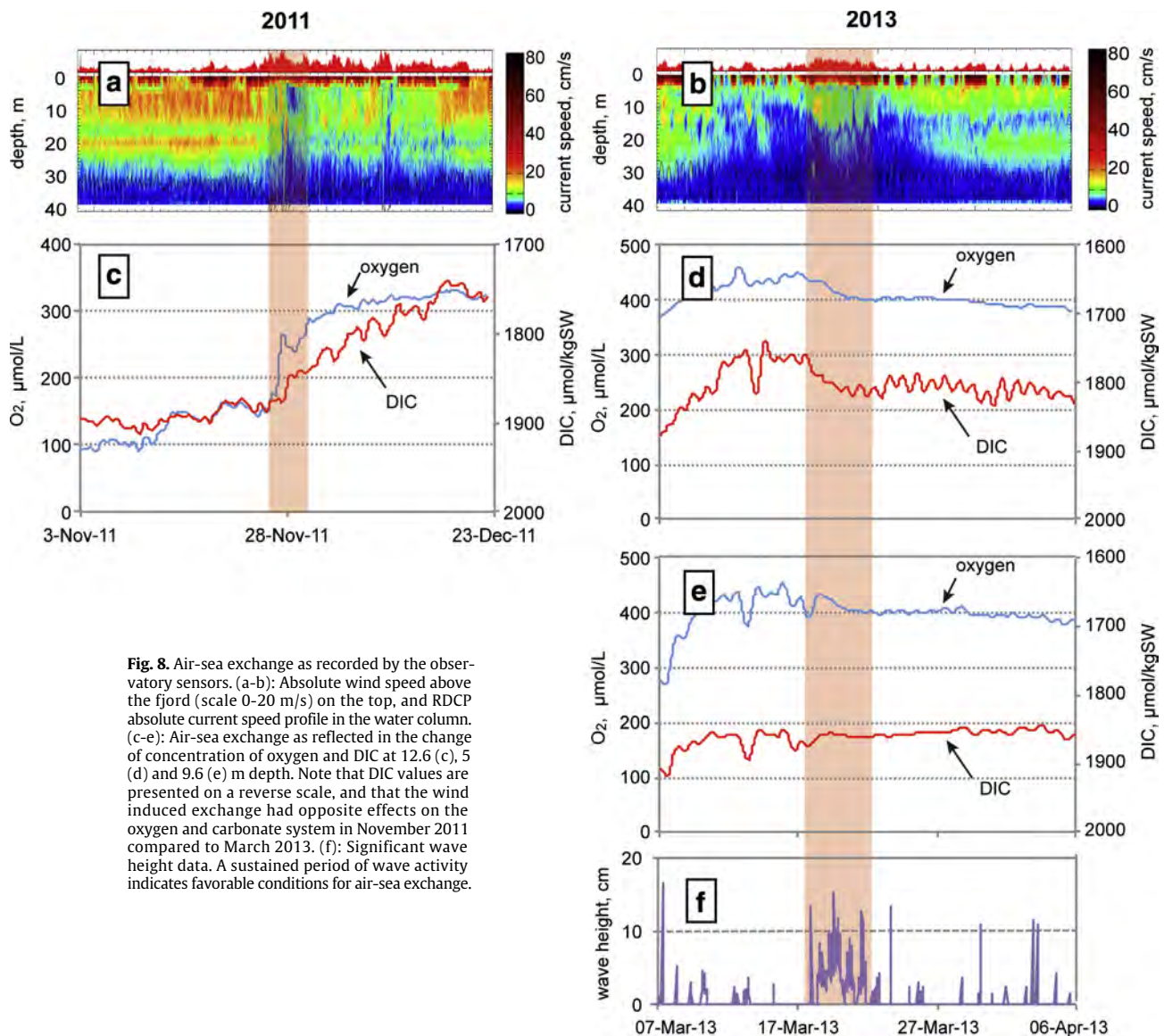


Fig. 8. Air-sea exchange as recorded by the observatory sensors. (a–b): Absolute wind speed above the fjord (scale 0–20 m/s) on the top, and RDCP absolute current speed profile in the water column. (c–e): Air-sea exchange as reflected in the change of concentration of oxygen and DIC at 12.6 (c), 5 (d) and 9.6 (e) m depth. Note that DIC values are presented on a reverse scale, and that the wind induced exchange had opposite effects on the oxygen and carbonate system in November 2011 compared to March 2013. (f): Significant wave height data. A sustained period of wave activity indicates favorable conditions for air-sea exchange.

5. Conclusions

We have used a cabled observatory and a stand-alone mooring to study the carbonate system in the upper part of the water column above the pycnocline in the Koljo Fjord, western Sweden, from September or October to April during two consecutive years. The combination of high frequency measurements of $p\text{CO}_2$, pH, O_2 , salinity, temperature, chlorophyll a, wave and acoustic particle measurements at multiple levels offered possibilities for deeper understanding and monitoring of physical, chemical and biological processes in the fjord, which would not have been possible by occasional sampling from a ship. This study has also demonstrated the advantages of using an observatory equipped with multiple sensors in doing continuous detailed studies of the marine carbonate system.

In this study $p\text{CO}_2$ was measured with a new type of compact optical sensor (Atamanchuk et al., 2014) that worked well, giving sufficient resolution and no significant drift, throughout these measurement periods. $p\text{CO}_2$ concentrations varied between approximately 210 and 940 μatm . During the same periods O_2 varied from about 80 to 470 $\mu\text{mol/L}$.

Biological processes were mainly responsible for slower and gradual changes of O_2 and $p\text{CO}_2$ including organic matter

degradation in autumn, and primary production in early spring. During winter a deepening of the mixed layer was observed, which resulted in gradual enrichment of the water column above the pycnocline with DIC. A vivid illustration of the timing of processes was achieved by plotting variations in O_2 and DIC on Redfield scaled plots.

Water column integrated NPP rates calculated from oxygen production rates at different depths during the spring blooms were 1.79 and 2.10 g C m^{-2} in 2012 and 2013, respectively. Difference in light availability, which limits primary production during this time of the year, explains the inter-annual variability. On a daily basis during the spring bloom period, these rates correspond to 71–161 $\text{mg C m}^{-2} \text{d}^{-1}$. These values agree with, or are in the lower end of, previously published daily NPP rates from the open Kattegat and the adjacent Gullmar Fjord (89–625 $\text{mg C m}^{-2} \text{d}^{-1}$), though the span is significant.

Acoustic reflections from the RDCP profiler helped to identify the start and duration of the spring bloom, which was also clearly detected by the O_2 , $p\text{CO}_2$, DIC and chlorophyll a measurements. On average production of OM during the bloom occurred in the ratio $\text{O}_2:\text{DIC} = -1.56$. Diffusive transport of oxygen, turbulent mixing and air-sea exchange

lead to biases in O₂:C ratios during primary production and thus non-biological components have to be carefully investigated and assessed.

As recorded by the sensors placed at different depths in surface and intermediate layers, the Koljo Fjord is dynamic and highly affected by seasonality. Short term variations, on the time scale of hours, were mainly induced by tidal oscillations and/or by periods of strong winds which lead to air–sea exchange in the surface layers and/or to occasional transport of DIC enriched and oxygen depleted water from below the pycnocline and/or from adjacent fjords.

In the future long-term measurements with high temporal resolution at the Koljo Fjord observatory will continue to contribute to the improved understanding of the characteristics of the Orust fjord system and will be used for validation of existing hydrographical models (Hansson et al., 2013; Friedrich et al., 2014). Highly spatially and temporally resolved multiparameter observations in the water column will allow for better understanding and more explicit description of biogeochemical and physical processes in complex systems like this fjord system on the west coast of Sweden.

Acknowledgments

This work was supported by SENSEnet (International sensor development network) – a Marie Curie Initial Training Network (ITN) funded by the European Commission Seventh Framework Programme under contract number PITN-GA-2009–237868. The installation of the Koljo Fjord cabled observatory was done in collaboration with C. Waldmann at MARUM, Bremen, and funded by the European Commission projects ESONET-NoE (contract number 036851), HYPOX (grant agreement number 226213) and EMSO (grant agreement number 211816). Support was obtained from Aanderaa Data Instruments (Bergen, Norway), YSI (Yellow Springs, USA) provided sensors and instruments, and the Michelsen Centre (Norway) funded the pCO₂ sensor calibrations and some sensor trials. Constructive comments from two anonymous reviewers helped us improve the manuscript.

References

- Aarup, T., 2002. Transparency of the North Sea and Baltic Sea – a Secchi depth data mining study. *Oceanologia* 44 (3), 323–337.
- Alvarez, M., Rios, A.F., Roson, G., 2002. Spatio-temporal variability of air–sea fluxes of carbon dioxide and oxygen in the Bransfield and Gerlache Straits during austral summer 1995–96. *Deep-Sea Res. Part II* 49, 643–662.
- Anderson, L.A., Sarmiento, J.L., 1994. Redfield ratios of remineralization determined by nutrient data analysis. *Glob. Biogeochem. Cycles* 8, 65–80.
- Andersson, L., Rydberg, L., 1988. Trends in nutrient and oxygen conditions within the Kattegat: effects of local nutrient supply. *Estuar. Coast. Shelf Sci.* 26, 559–579.
- Atamanchuk, D., Tengberg, A., Thomas, P.J., Hovdenes, J., Apostolidis, A., Huber, C., et al., 2014. Performance of a lifetime-based optode for measuring partial pressure of carbon dioxide in natural waters. *Limnol. Oceanogr. Methods* 12, 63–73.
- Bates, N.R., 2007. Interannual variability of the oceanic CO₂ sink in the subtropical gyre of the North Atlantic Ocean over the last 2 decades. *J. Geophys. Res. C Oceans* 112 (9), C09013.
- Billett, D.S.M., Bett, B.J., Reid, W.D.K., Boorman, B., Priede, I.G., 2010. Long-term change in the abyssal NE Atlantic: the ‘Amperima Event’ revisited. *Deep-Sea Res. Part II* 57 (15), 1406–1417.
- Bozec, Y., Thomas, H., Schiettecatte, L.-S., Borges, A.V., Elkalay, K., de Baar, H.J.W., 2006. Assessment of the processes controlling the seasonal variations of dissolved inorganic carbon in the North Sea. *Limnol. Oceanogr.* 51, 2746–2762.
- Byrne, R.H., Yao, W., Kaltenbacher, E.A., Waterbury, R.D., 2000. Construction of a compact spectrofluorometer/spectrophotometer system using a flexible liquid core waveguide. *Talanta* 50, 1307–1312.
- Byrne, R.H., Liu, X., Kaltenbacher, E.A., Sell, K., 2002. Spectrophotometric measurement of total inorganic carbon in aqueous solutions using a liquid core waveguide. *Anal. Chim. Acta* 451 (2), 221–229.
- Carrillo, C.J., Smith, R.C., Karl, D.M., 2004. Processes regulating oxygen and carbon dioxide in surface waters west of the Antarctic Peninsula. *Mar. Chem.* 84, 61–179.
- DeGrandpre, M.D., Hammar, T.R., Smith, S.P., Sayles, F.L., 1995. In situ measurements of seawater CO₂. *Limnol. Oceanogr.* 40, 969–975.
- DeGrandpre, M.D., Hammar, T.R., Wallace, D.W.R., Wirrick, C.D., 1997. Simultaneous mooring-based measurements of seawater CO₂ and O₂ off Cape Hatteras, North Carolina. *Limnol. Oceanogr.* 42, 21–28.
- DeGrandpre, M.D., Hammar, T.R., Wirrick, C.D., 1998. Short-term pCO₂ and O₂ dynamics in California coastal waters. *Deep-Sea Res. Part II* 45 (8–9), 1557–1575. [http://dx.doi.org/10.1016/S0967-0645\(98\)80006-4](http://dx.doi.org/10.1016/S0967-0645(98)80006-4).
- Dickson, A.G., Millero, F.J., 1987. A comparison of the equilibrium constants for the dissociation of carbonic acid in seawater media. *Deep-Sea Res. Part A* 34, 1733–1743.
- Dickson, Riley, 1978. *Mar. Chem.* 6, 77–85.
- Dore, J.E., Lukas, R., Sadler, D.W., Church, M.J., Karl, D.M., 2009. Physical and biogeochemical modulation of ocean acidification in the central North Pacific. *Proc. Natl. Acad. Sci. U. S. A.* 106 (30), 12235–12240.
- Emerson, S.R., Hedges, J.L., 2008. *Chemical Oceanography and the Marine Carbon Cycle*. Cambridge University Press, New York.
- Fiedler, B., Fietzek, P., Vieira, N., Silva, P., Bittig, H.C., Körtzinger, A., 2013. In situ CO₂ and O₂ measurements on a profiling float. *J. Atmos. Ocean. Technol.* 30 (1), 112–126.
- Friederich, G.E., Brewer, P.G., Herliou, R., Chavez, F.P., 1995. Measurement of sea surface partial pressure of CO₂ from a moored buoy. *Deep-Sea Res.* 42, 1175–1186.
- Friedrich, J., Janssen, F., Aleynik, D., Bange, H.W., Boltacheva, N., Çağatay, M.N., et al., 2014. Investigating hypoxia in aquatic environments: diverse approaches to addressing a complex phenomenon. *Biogeosciences* 10, 12655–12772.
- Gago, J., Gilcoto, M., Perez, F.F., Rios, A.F., 2003. Short-term variability of fCO₂ in seawater and air–sea CO₂ fluxes in a coastal upwelling system (Ria de Vigo, NW Spain). *Mar. Chem.* 80, 247–264.
- Goyet, C., Snover, A.K., 1993. High-accuracy measurements of total dissolved inorganic carbon in the ocean: comparison of alternate detection methods. *Mar. Chem.* 44 (2–4), 235–242.
- Hansson, D., Stigebrandt, A., Liljebadh, B., 2013. Modeling the Orust fjord system on the Swedish west coast. *J. Mar. Syst.* 111–112, 1–10.
- Haraldsson, C., Anderson, L.G., Hasselov, M., Hulth, S., Olsson, K., 1997. Rapid, high-precision potentiometric titration of alkalinity in ocean and sediment pore waters. *Deep-Sea Res.* 44, 2031–2044.
- Hartman, S.E., Larkin, K.E., Lampitt, R.S., Lankhorst, M., Hydes, D.J., 2010. Seasonal and inter-annual biogeochemical variations in the Porcupine Abyssal Plain 2003–2005 associated with winter mixing and surface circulation. *Deep-Sea Res. Part II* 57 (15), 1303–1312.
- Hartman, S.E., Lampitt, R.S., Larkin, K.E., Pagnani, M., Campbell, J., Gkrizalis, et al., 2012. The Porcupine Abyssal Plain fixed-point sustained observatory (PAP-SO): variations and trends from the Northeast Atlantic fixed-point time series. *ICES J. Mar. Sci.* 69 (5), 776–783.
- Heilmann, J.P., Richardson, K., Ærtebjerg, G., 1994. Annual distribution and activity of phytoplankton in the Skagerrak–Kattegat frontal region. *Mar. Ecol. Prog. Ser.* 112, 213–223.
- Hood, E.M., Merlivat, L., Johannessen, T., 1999. Variations of fCO₂ and air–sea flux of CO₂ in the Greenland Sea gyre using high-frequency time series data from CARIACO drift buoys. *J. Geophys. Res.* 104, 20571–20583.
- Johnson, K.S., 2010. Simultaneous measurements of nitrate, oxygen and carbon dioxide on oceanographic moorings: observing the Redfield ratio in real-time. *Limnol. Oceanogr.* 55, 615–627.
- Johnson, K.S., Needoba, J.A., Riser, S.C., Showers, W.J., 2007. Chemical sensor networks for the aquatic environment. *Chem. Rev.* 107 (2), 623–640.
- Johnson, Kenneth S., Coletti, Luke J., Jannasch, Hans W., Sakamoto, Carole M., Swift, Dana, Riser, Stephen C., 2013. Long-term nitrate measurements in the ocean using the in situ ultraviolet spectrophotometer: sensor integration into the Apex profiling float. *J. Atmos. Ocean. Technol.* 30, 1854–1866.
- Körtzinger, A., Send, U., Wallace, D.W.R., Karstensen, J., DeGrandpre, M.D., 2008a. Seasonal cycle of O₂ and pCO₂ in the central Labrador Sea: atmospheric, biological, and physical implications. *Glob. Biogeochem. Cycles* 22, GB1014. <http://dx.doi.org/10.1029/2007GB003029>.
- Körtzinger, A., Send, U., Lampitt, R.S., Hartman, S., Wallace, D.W.R., Karstensen, J., et al., 2008b. The seasonal pCO₂ cycle at 49°N/16.5°W in the northeastern Atlantic Ocean and what it tells us about biological productivity. *J. Geophys. Res.* 113, C04020. <http://dx.doi.org/10.1029/2007JC004347>.
- Kuliński, K., Schneider, B., Hammer, K., Machulik, U., Schulz-Bull, D., 2014. The influence of dissolved organic matter on the acid–base system of the Baltic Sea. *J. Mar. Syst.* 132, 106–115.
- Kuss, J., Roeder, W., Wlost, K.-P., DeGrandpre, M.D., 2006. Time series of surface water CO₂ and oxygen measurements on a platform in the central Arkona Sea (Baltic Sea): seasonality of uptake and release. *Mar. Chem.* 101, 220–232.
- Lee, K., Millero, F.J., Byrne, R.H., Feely, R.A., Wanninkhof, R., 2000. The recommended dissociation constants for carbonic acid in seawater. *Geophys. Res. Lett.* 27 (2), 229–232.
- Lee, K., Tong, L.T., Millero, F.J., Sabine, C.L., Dickson, A.G., Goyet, C., et al., 2006. Global relationships of total alkalinity with salinity and temperature in surface waters of the world’s oceans. *Geophys. Res. Lett.* 33, L19605.
- Lewis, E., Wallace, D.W.R., 1998. Program Developed for CO₂ System Calculations. ORNL/CDIAC-105. Carbon Dioxide Information Analysis Center, Oak Ridge National Laboratory, U.S. Department of Energy, Oak Ridge (TN).
- Lindahl, O., Andersson, L., Belgrano, A., 2009. Primary Phytoplankton Productivity in the Gullmar Fjord, Sweden: an Evaluation of the 1985–2008 Time Series. Swedish Environmental Protection Agency, Stockholm.
- Mehrbach, C., Culberson, C.H., Hawley, J.E., Pytkowicz, R.M., 1973. Measurement of the apparent dissociation constants of carbonic acid in seawater at atmospheric pressure. *Limnol. Oceanogr.* 8, 897–907.
- Millero, F.J., 2007. The marine inorganic carbon cycle. *Chem. Rev.* 107 (2), 308–341.
- Muller, F.L.L., Bleie, B., 2008. Estimating the organic acid contribution to coastal seawater alkalinity by potentiometric titrations in a closed cell. *Anal. Chim. Acta.* 619, 183–191.
- Nordberg, K., Filipsson, H.L., Gustafsson, M., Harland, R., Roos, P., 2001. Climate, hydrographic variations and marine benthic hypoxia in Koljö fjord, Sweden. *J. Sea Res.* 46, 187–200. [http://dx.doi.org/10.1016/S1385-1101\(01\)00084-3](http://dx.doi.org/10.1016/S1385-1101(01)00084-3).
- O’Sullivan, D.W., Millero, F.J., 1998. Continual measurement of the total inorganic carbon in surface seawater. *Mar. Chem.* 60 (1–2), 75–83.

- Redfield, A.C., 1934. On the proportions of organic derivations in seawater and their relation to the composition of plankton. In: Daniel, R.J. (Ed.), James Johnstone Memorial Volume. University Press of Liverpool, Liverpool, pp. 177–192.
- Redfield, A.C., Ketchum, B.H., Richards, F.A., 1963. The influence of organisms on the composition of seawater. In: Hill, M.N. (Ed.), *The Sea* vol. 2. John Wiley, New York, pp. 26–77.
- Saderne, V., Fietzek, P., Herman, P.M.J., 2013. Extreme variations of pCO₂ and pH in a macrophyte meadow of the Baltic Sea in summer: evidence of the effect of photosynthesis and local upwelling. *PLoS ONE* 8 (4), e62689.
- Santana-Casiano, J.M., González-Dávila, M., Rueda, M.-J., Llinás, O., González-Dávila, E.-F., 2007. The interannual variability of oceanic CO₂ parameters in the northeast Atlantic subtropical gyre at the ESTOC site. *Glob. Biogeochem. Cycles* 21 (1), GB1015.
- Shadwick, E.H., Thomas, H., Azetsu-Scott, K., Greenan, B.J.W., Head, E., Horne, E., 2011. Seasonal variability of dissolved inorganic carbon and surface water pCO₂ in the Scotian Shelf region of the Northwestern Atlantic. *Mar. Chem.* 124 (1–4), 23–37.
- Shitashima, K., Kyo, M., Koike, Y., Henmi, H., 2002. Development of in-situ pH sensor using ISFET. *Proceed of the 2002 Int Symp on Underwater Technology*. IEEE, pp. 106–108 (02EX556).
- Stigebrandt, A., 1991. Computations of oxygen fluxes through the sea surface and the net production of organic matter with application to the Baltic and adjacent seas. *Limnol. Oceanogr.* 36 (3), 444–454.
- Tengberg, A., Hovdenes, J., Andersson, H.J., Brocandel, O., Diaz, R., Hebert, D., et al., 2006. Evaluation of a lifetime-based optode to measure oxygen in aquatic systems. *Limnol. Oceanogr. Methods* 4, 7–17.
- Wang, Z.A., Liu, X., Byrne, R.H., Wanninkhof, R., Bernstein, R.E., Kaltenbacher, E.A., et al., 2007. Simultaneous spectrophotometric flow-through measurements of pH, carbon dioxide fugacity, and total inorganic carbon in seawater. *Anal. Chim. Acta* 596 (1), 23–36.
- Wanninkhof, R., 1992. Relationship between wind speed and gas exchange over the ocean. *J. Geophys. Res.* 97, 7373–7382.
- Wesslander, K., Hall, P.O.J., Hjalmarsson, S., Lefevre, D., Omstedt, A., Rutgersson, A., et al., 2011. Observed carbon dioxide and oxygen dynamics in a Baltic Sea coastal region. *J. Mar. Syst.* 86, 1–9.
- Zhai, W.D., Dai, M., Cai, W.-J., 2009. Coupling of surface pCO₂ and dissolved oxygen in the northern South China Sea: impacts of contrasting coastal processes. *Biogeosciences* 6, 2589–2598. <http://dx.doi.org/10.5194/bg-6-2589-2009>.